American Mineralogist, Volume 75, pages 120–134, 1990

Role of Al in depolymerized, peralkaline aluminosilicate melts in the systems Li_2O-Al_2O_3-SiO_2, Na_2O-Al_2O_3-SiO_2, and K_2O-Al_2O_3-SiO_2

Bjorn O. Mysen

Geophysical Laboratory, Carnegie Institution of Washington, 2801 Upton Street, N.W., Washington, D.C. 20008, U.S.A.

Abstract

The structures of quenched (temperature quenched from 1400 °C) alkali (K, Na, and Li) aluminosilicate melts compositionally on tetrasilicate ($M_2Si_4O_9$)–tetra-aluminate [$M_2(MAl)_4O_9$] joins (M = Li, Na, and K) have been studied with Raman spectroscopy. In these melts, Al^{3+} is a network-former charge-balanced with K, Na, and Li, and the bulk melt ratio of nonbridging oxygens per tetrahedrally coordinated cations (NBO/T) is 0.5.

In the Al-free end-member quenched melts, structural units with NBO/Si = 0 (SiO_2), 1 ($Si_2O_5^{2-}$), and 2 (SiO_3^{2-}) coexist with the mole fractions X_{SiO_2} and $X_{SiO_3^{2-}}$ increasing and $X_{Si_2O_5^{2-}}$ decreasing in the order Li > Na > K. Structural units less polymerized than that of SiO_3^{2-} were not detected. Substitution of Al for Si with concomitant alkali charge-balancing enhances the abundance of fully polymerized units (and units with NBO/T = 2).

The reaction T_2O_5 ($2Q^3$) ↔ TO_3 (Q^2) + TO_2 (Q^4) (T = Al + Si and Q^n indicates the degree of polymerization, where $n = 4 - NBO/T$) describes the anionic equilibrium in these melts. In Al-free end-member composition melts, this equilibrium is shifted to the right as the ionic radius of the network-modifying cation decreases. Increasing Al/(Al + Si) also shifts this reaction to the right. The extent of this shift depends on the charge-balancing cation for tetrahedrally coordinated Al and increases in the order Li < Na < K.

Introduction

Al and Si are the principal network-forming cations in magmatic silicate liquids. Al differs from Si, however, in that when in tetrahedral coordination, it requires charge-balancing with metal cations such as alkali metals or alkaline earths. In felsic magmas (e.g., rhyolite and rhyodacite), alkali metals are the predominant charge-balancing cations, whereas in more mafic compositions (e.g., basaltic liquid), some of the alkaline earths (Mg and Ca, and possibly also Fe^{2+}) are also associated with Al^{3+} in tetrahedral coordination (Mysen, 1987).

Physical and chemical properties of magmatic liquids vary widely depending on their composition. The compositional variations, in turn, govern the melt structure. The degree of polymerization (nonbridging oxygen per tetrahedrally coordinated cations; NBO/T) exerts a major control on many of these properties. For example, in compositions ranging from binary metal oxide–silica to complex natural magmatic liquids, molar volume and isothermal viscosity increase with increasing melt polymerization (decreasing NBO/T) (e.g., Bockris et al., 1955; Urbain et al., 1982; Robinson, 1969; Bottinga et al., 1983; see also Mysen, 1987, for review of this information).

A major structural unit in natural magmatic liquids is the fully polymerized unit (TO_2; T = Al + Si with appropriate charge-balancing of tetrahedrally coordinated Al^{3+}). For melt compositions along aluminate–silica joins ($MAlO_2$–SiO_2 and $M_{0.5}AlO_2$–SiO_2); only TO_2 units occur. In these compositions, both the Al content and the type of charge-balancing cation affect melt properties such as liquidus temperatures, viscosity, compressibility, and heat of mixing (e.g., Ryerson, 1985; Urbain et al., 1982; Seifert et al., 1982; Navrotsky et al., 1985). The type of network-modifier affects both melt structure and melt properties. For example, the heat of mixing of melts on metal oxide–silica joins increases (becomes less negative) with increasing Z/r^2 of the metal (Eliezer et al., 1978, 1979), and the melt viscosity increases (Bockris et al., 1955).

Natural magmatic liquids are aluminous and contain nonbridging oxygen. For example, typical tholeiitic melts have NBO/T between 0.7 and 0.9, the range for andesitic melts is between 0.2 and 0.4, and that for rhyolites is between 0.05 and 0.15. Their Al/(Al + Si) values are between 0.2 and 0.3 (Mysen, 1987). Metal cations in such melts may act in part as charge-balancing cations and in part as network modifiers. From spectroscopic studies in simple binary metal oxide–silica systems, it has been shown that several structural units coexist in depolymerized aluminosilicate melts (Virgo et al., 1980; Mysen et al., 1980; Matson et al., 1983; Murdoch et al., 1985; Stebbins, 1987). In peralkaline aluminosilicate melts, Al is distributed between these structural units (e.g., Mysen et al., 1981, 1985; Domine and Piriou, 1986; Oestrike and Kirkpatrick, 1988). This distribution is not random and, in addition to pressure and temperature (Mysen et al.,

0003–004X/90/0102–0120$02.00

1985), probably is also a function of Al/(Al + Si) and which metal cations are in the system (Mysen et al., 1981). In order to characterize possible relationships between structure and properties in peralkaline aluminosilicate melts, these compositional effects on the melt structure must be addressed. In this report, melts containing alkali metals with Z/r^2 between 0.57 (K) and 1.7 (Li) and having Al/(Al + Si) between 0 and 0.4 have been employed to determine the effects on melt structure.

Experimental methods

Starting materials

Starting materials were mixtures of Li_2CO_3, Al_2O_3, and SiO_2; Na_2CO_3, Al_2O_3, and SiO_2; and K_2CO_3, Al_2O_3, and SiO_2 on the composition joins between the tetrasilicate ($M_2Si_4O_9$) and tetra-aluminate ($M_2(MAl)_4O_9$), where M = alkali metal. Provided that Al^{3+} is in tetrahedral coordination, exchange of Al^{3+} for Si^{4+} in melts on these joins does not affect the bulk melt polymerization (NBO/T = 0.5).

The samples were taken from 50-g liquid mixtures also used for viscosity measurements in another study (D. B. Dingwell, in preparation). Part of each mixture was poured onto a cold surface after the mixture had been stirred for several hours in a concentric cylinder viscometer. About 50 mg of the material was then returned to the experimental temperature in a vertical quench furnace and then quenched in water. Although the quenching rates cannot be measured accurately with this method, the cooling rates from experimental temperatures (1400 °C) to about 700 °C were about 500 °C/s. Chemical compositions of the glasses are given in Table 1.

Table 1. Chemical composition of glasses

	SiO_2	Al_2O_3	K_2O	Na_2O	Li_2O
KS4	72.42	—	27.58	—	—
$KS4(KA4)_5$	67.86	2.96	29.18	—	—
$KS4(KA4)_{10}$	62.24	5.87	31.90	—	—
$KS4(KA4)_{15}$	57.71	8.54	33.76	—	—
$KS4(KA4)_{20}$	53.36	11.22	35.41	—	—
$KS4(KA4)_{25}$	49.31	13.48	37.21	—	—
NS4	80.33	—	—	19.68	—
$NS4(NA4)_5$	75.22	3.48	—	21.31	—
$NS4(NA4)_{10}$	70.21	6.45	—	23.34	—
$NS4(NA4)_{20}$	61.37	12.18	—	26.45	—
$NS4(NA4)_{30}$	53.03	16.78	—	30.20	—
$NS4(NA4)_{40}$	44.67	21.71	—	33.63	—
LSR	89.20	—	—	—	10.80
$LS4(LA4)_{10}$	79.59	7.36	—	—	13.04
$LS4(LA4)_{20}$	70.46	14.61	—	—	14.93

Note: Chemical analyses from D. B. Dingwell (in preparation). Analyses courtesy of Michel Pichavant by ICP.

Spectroscopic analysis

Structural information was derived from Raman spectra of the quenched melts with an automated Raman spectrometer system described by Mysen et al. (1982a). The 514-nm line of an Ar^+ ion laser operating at 2–4 W was used for sample excitation. Briefly, this system consists of an LSI 11 minicomputer interfaced with a photon counter and the slit and wavelength drives of the Raman spectrometer.

The spectra were corrected for temperature- and frequency-dependent scattering intensity (e.g., Long, 1977) prior to statistical analysis. The intensities in all reported spectra are normalized to the data point of the greatest absolute intensity. The background was subtracted from the uncorrected spectra by least-squares fitting of a line (typically an exponential curve) through the data points at frequencies greater than those where Raman scattering was observed. As discussed in detail elsewhere (Seifert et al., 1981a, 1982; Mysen et al., 1982a), the curve fitting was carried out on a completely statistical basis with the method of minimization of least squares described by Davidon (1966), Fletcher and Powell (1963), and Powell (1964a, 1964b). Upon convergence, the minimum value of χ^2 and maximum randomness in residual distribution are obtained. All line parameters (frequency, half-width, and intensity) as well as the number of lines are independent variables in the fitting routine.

Compared with the Raman spectra of crystalline materials, the vibrational modes in amorphous materials can be expected to be broader owing to thermal distribution of local geometries and vibrational coupling. There is no a priori test that can be performed to document the line shape of the broad Raman bands of amorphous materials. As suggested elsewhere (e.g., Walrafen, 1967; Hartwig, 1977; Mysen et al., 1982a; Seifert et al., 1982; McMillan et al., 1982; McKeown et al., 1984), the Raman spectra of amorphous materials such as silicate glass are best fitted with bands of Gaussian line shape. In view of the suggestion from both Raman and NMR spectroscopy (e.g., Virgo et al., 1980; Mysen et al., 1982b; Matson et al., 1983; Murdoch et al., 1985; Stebbins, 1987, 1988; Brandriss and Stebbins, 1988) that depolymerized silicate melts can be described in terms of several coexisting structural units (or species), the Raman spectrum of such melts will be complex, and individual bands in the raw spectra are cumulative envelopes. Thus, a test of various line shapes (and perhaps whether or not individual lines might not be symmetric) for such materials against the overall topology of a spectrum cannot be easily accomplished. However, the high-frequency portion of the spectrum of vitreous SiO_2 is comparatively simple. For this reason, Mysen and Virgo (1985) undertook a detailed study of spectra of vitreous silica and used both Gaussian and Lorentzian line shapes (and mixtures of the two) in the analysis of the spectral information. Those authors also found that Gaussian line shapes provided the most satisfactory results.

The spectra under consideration here (see Fig. 1, for example, but see also below for more detailed description and analysis) are somewhat more complex than the spectrum of SiO_2, but a similar analysis is fruitful to illustrate how some of the principal variables in the fitting procedure can affect the results. There are three variables of major interest in the fitting procedure. These are (1) the

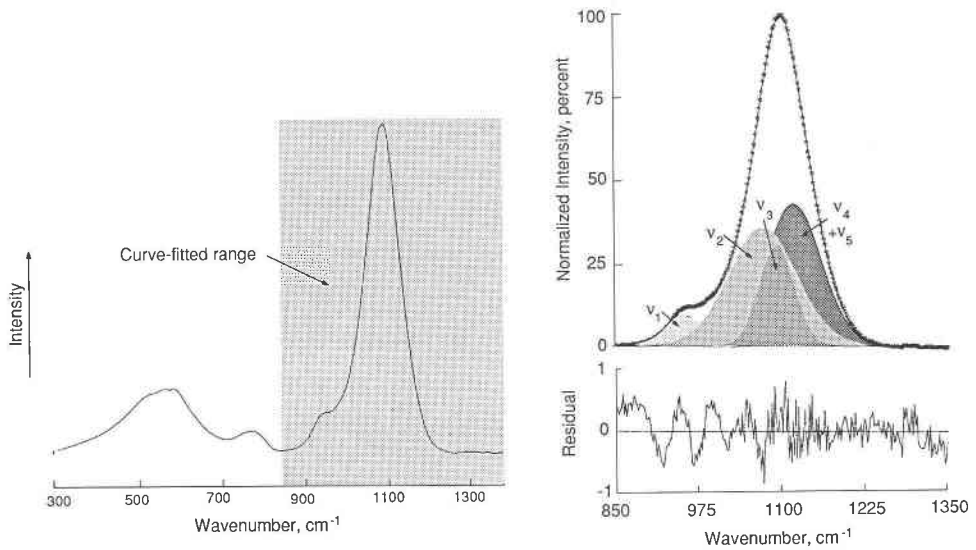

Fig. 1. Raman spectrum of composition $NS4(NA4)_{10}$ and curve-fitted high-frequency portion of spectrum.

line shapes, (2) the number of lines to be fitted, and (3) whether the minima in χ^2 are global or regional.

The high-frequency envelope (850–1350 cm^{-1}) of the spectrum of composition $NS4(NA4)_{10}$ [90 mol% $Na_2Si_4O_9$ component and 10 mol% $Na_2(NaAl)_4O_9$ component] (Fig. 1) will be used in this example. The fits resulting from ten different sets of input variables (frequency, ν, full width at half height, ω, and intensity, I) are shown in Table 2 together with the resulting values of χ^2. As can be seen from the results in that table, widely different input parameters have small or negligible effect on the fitted line parameters, and the values of χ^2 from the individual fits vary by less than 3%.

When fitting the spectrum with more than four lines, statistically insignificant improvements in χ^2 result (Table 2). Moreover, the areas of the additional bands (relative to the total area of the high-frequency envelope) are negligibly small (0.25% ± 0.3% for the fifth band in the five-line fit and 0.25% ± 0.5% and 0.03% ± 0.3% for the two additional bands in the six-line fit). By reducing the number of bands below four, the values of χ^2 increase rapidly (Table 2).

From the analysis above, it is concluded that for Gaussian line shapes, four lines provide the best fit to the high-frequency envelope. Fewer lines greatly diminish the goodness-of-fit, and more lines do not improve it. Alternative line shapes such as Lorentzian have been suggested (e.g., Barker and Sievers, 1975). The fits with 0% and 10% Lorentzian component are indistinguishable, but with a further increase in the fraction of a Lorentzian component, the values of χ^2 (Fig. 2) increase very rapidly. From similar analyses of line shapes of Raman bands of spectra of samples in the systems $CaO\text{-}SiO_2$, $NaAlO_2\text{-}SiO_2$, $CaAl_2O_4\text{-}SiO_2$, and $MgAl_2O_4\text{-}SiO_2$ (Mysen et al., 1982a; Seifert et al., 1982), the same conclusions were reached.

An additional test on the suitability of this fitting procedure and the suggested symmetric Gaussian line shape of the Raman spectra of quenched silicate melts is possible. Because abundance data of individual structural units in simple binary metal oxide–silica melts (previously only available from the Raman data) have recently been reported from ^{29}Si NMR analyses (Stebbins, 1987, 1988; Schneider et al., 1987; Brandriss and Stebbins, 1988), the abundance data from Raman spectra fitted with symmetric Gaussian lines can now be compared with the abundance data from ^{29}Si NMR spectroscopy. The glasses used in both the Raman and NMR studies were temperature-quenched at approximately the same rates. Thus, the structures deduced from those spectra most probably were frozen in at approximately the same temperature (see also detailed discussion below on the subject of temperature and temperature-quenching). These data compare favorably (Fig. 3). In Figure 3, the original Raman spectra used to calculate the molar abundances were those reported by Mysen et al. (1982b). It is noted, however, that the mole fractions shown in Figure 3 were derived by a somewhat different method than that used in the original report, and there are some differences in the detailed abundances. In view of these differences, the procedures and uncertainties associated with the two methods need to be assessed in some detail.

In both methods, relative intensity ratios of $Si\text{-}O^-$ stretch bands (the high-frequency envelopes between about 800 and 1250 cm^{-1}) were used. In the original report (Mysen et al., 1982b; but see also Mysen et al., 1982a, and Seifert et al., 1981a, for more detailed description), normalized Raman cross sections, a_i, were related to normalized area ratios from the Raman spectra, A_i, of a Raman band, i, relative to all the bands in the high-frequency envelope. With the number of nonbridging oxygens in the structural unit, i, denoted n_i, the overall degree of polymerization of a melt could be described with the mass balance:

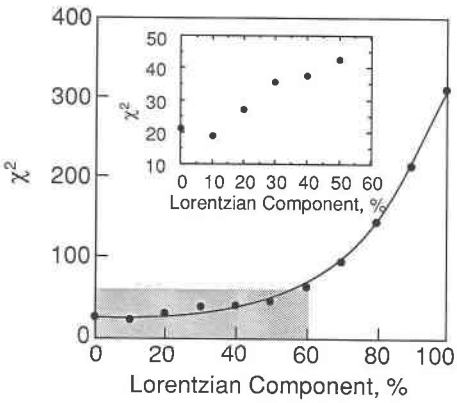

Fig. 2. Relationships between percentage Lorentzian component for mixed line shapes (between Gaussian and Lorentzian) and values of χ^2 of converged fits with four lines fitted to the high-frequency envelope of spectrum of composition $NS4(NA4)_{10}$.

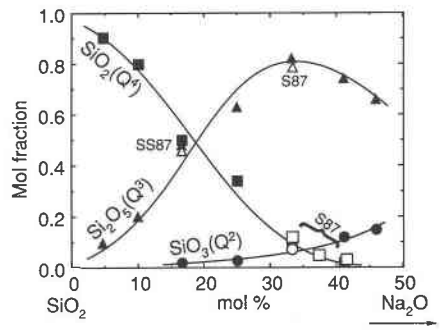

Fig. 3. Mole fractions of structural units in quenched melts on the join Na_2O–SiO_2 from Raman spectroscopy are compared with mole fractions of structural units of various quenched sodium silicate melts from ^{29}Si NMR reported by Stebbins (1987) (denoted S87) and Schneider et al. (1987) (denoted SS87). Dark symbols, from Raman spectroscopy; open symbols, from NMR spectroscopy. Triangles, $Si_2O_5^{2-}$ units; squares, SiO_2 units; circles, SiO_3^{2-} units.

$$\sum_{i=1}^{I} a_i A_i n_i = \text{NBO/T}. \quad (1)$$

An additional mass-balance,

$$\sum_{i=1}^{I} a_i A_i = 1, \quad (2)$$

was also used. In order to solve for the cross section, a_i, a set of equations obtained with a number of spectra equal to or larger than the number of structural units of samples with different bulk degree of polymerization, NBO/T, was used (Seifert et al., 1981a; Mysen et al., 1981a, 1982b). In view of the errors associated with the area determinations in each spectrum (10%–20%, relative), these equations were solved for the normalized cross sections by least-squares minimization.

In solving Equation 1 for a_i, four or more equations were used in the original method for determination of Raman cross sections, and the error in the resulting values of the cross sections is 30% or more even for the statistically most accurate spectra. Thus, in using such values to compute the mole fraction of a given structural unit for an unknown sample, the relative error in the resulting value probably was at least between 30% and 40%. It is suggested that the apparent discrepancy between the abundance data from Mysen et al. (1982b) and those from ^{29}Si NMR reported, for example, by Stebbins

TABLE 2. Results of (1) different variable input parameters and (2) different numbers of lines fitted to high-frequency envelope for curve fitting of spectrum of sample $NS4(NA4)_{10}$ quenched from 1400 °C

Band	Input parameters*			Output parameters**					
	Range			Range			Average (n = 10)		
	ν (cm^{-1})	ω (cm^{-1})	I (%)	ν (cm^{-1})	ω (cm^{-1})	I (%)	ν (cm^{-1})	ω (cm^{-1})	I (%)
n_1	930–980	20–45	5.0–15.0	950–954	40–42	8.6–9.6	952 ± 1	41 ± 1	9.2 ± 0.3
n_2	1040–1090	40–75	25–50	1082–1091	70–76	31–39	1086 ± 5	71 ± 2	33 ± 5
n_3	1060–1110	30–50	20–64	1094–1101	34–36	25–31	1100 ± 2	35 ± 1	28 ± 3
n_4	1100–1150	40–70	20–50	1119–1134	57–63	46–56	1121 ± 6	61 ± 2	49 ± 4

	Range	Average (n = 10)
χ^2	21.3–22.0	21.6 ± 0.3

No. of lines	χ^2	Comment
2	389.8	
3	29.5	
4	21.3	
5	19.9	New line at 898 cm^{-1}, area = 0.25% ± 0.3% of total area
6	19	New lines at 885 cm^{-1}, area = 0.25% ± 0.5% of total area, and at 1226 cm^{-1}, area = 0.03% ± 0.3% of total area

Note: Symbols are ν, frequency of band; ω, full width at half height; I, intensity of band relative to the maximum intensity in the fitted envelope.
* Input parameters are the initial values of the line parameters used in the fitting routine.
** Output parameters are the fitted values of the line parameters upon convergence.

TABLE 3. Mole fraction of structural units for NS2NA15 composition melt

Species type	Quenched melt	800 °C	1000 °C	1100 °C
TO_2 (Q^4)	0.05 ± 0.01	0.10 ± 0.02	0.11 ± 0.02	0.16 ± 0.02
T_2O_5 (Q^3)	0.80 ± 0.14	0.80 ± 0.13	0.78 ± 0.13	0.68 ± 0.12
TO_3 (Q^2)	0.05 ± 0.01	0.10 ± 0.02	0.11 ± 0.02	0.16 ± 0.02

Note: Original Raman spectra reported by Seifert et al. (1981b), but fitted here for the present purposes. Bulk-melt NBO/T = 1.0, Al/(Al + Si) = 0.15.

(1987), could be reconciled by taking into account the large errors in the original data from Raman spectroscopy.

It is evident from the analysis above that the use of Raman spectroscopy to deduce concentrations of structural units requires a more accurate computational method than that suggested earlier (Seifert et al., 1981a; Mysen et al., 1982a, 1982b), and in this paper a simpler approach has been adopted. This method relies on the premise that under certain compositional circumstances, only one depolymerized structural unit can be detected in a melt. Such spectra can then be used to calibrate intensities (areas) of diagnostic Raman bands. For example, on the join Na_2O–SiO_2, for melts equal to or more polymerized than that of $Na_2O \cdot 9SiO_2$ (NS9) (see Mysen et al., 1982b, for spectra), only units with one nonbridging oxygen per Si can be detected ($Si_2O_5^{2-}$ or Q^3 units). For the Raman spectrum of a melt of NS9 composition, the intensity (area) ratio of the 1100 cm^{-1} antisymmetric stretch band ($Si_2O_5^{2-}$ or Q^3 units with 1 nonbridging oxygen per Si) relative to the Si-O^0 stretch band from bridging oxygen bonds, averaging near 1150 cm^{-1}, can then be converted to a measure of the abundance of these structural units. Composition NS9 has NBO/Si = 0.2, and the area ratio of the Raman bands $[A_{1100}/(A_{1100} + A_{1150})$, where A = area] is 0.23. The area ratio requires a correction factor of 0.89, therefore, to be a quantitative expression of the abundance of $Si_2O_5^{2-}$ (Q^3) units in the melt. With the fitting errors in that spectrum, the error in the correction factor is about 14%. In the K_2O-SiO_2 system (see below for detailed spectral discussion), the KS4 ($K_2O \cdot 4SiO_2$) spectrum exhibits no evidence of units more depolymerized than $Si_2O_5^{2-}$, and a similar procedure yields a correction factor of 0.85 ± 0.12. Thus, within the error of the analysis, these correction factors appear independent of composition.

For melts where the spectra also indicate the presence of other structural unites, the abundance of the second depolymerized units can be determined by simple mass balance of the nonbridging oxygens. For example, in sodium disilicate melts (bulk NBO/Si = 1), SiO_2, $Si_2O_5^{2-}$, and SiO_3^{2-} units can be detected (e.g., Mysen et al., 1982b; Matson et al., 1983; Stebbins, 1987). The abundance of $Si_2O_5^{2-}$ units, $X_{Si_2O_5^{2-}}$, is computed with the procedure above, and that of the SiO_3^{2-} units (which have two nonbridging oxygens per Si) is

$$X_{SiO_3^{2-}} = (NBO/T - X_{Si_2O_5^{2-}})/2. \quad (3)$$

The procedure outlined above was used to calculate the abundances in Figure 3. As can be seen from the comparison with the data on quenched melts from ^{29}Si NMR spectroscopy by Schneider et al. (1987) and Stebbins (1987), the results from the two methods agree well within the statistical uncertainties.

On the basis of the discussion above and the agreement between results from Raman and NMR spectroscopy, it is suggested, therefore, that the analysis of the Raman spectra employed here, using symmetric lines of Gaussian shape, is a reasonable approach to deconvolution of Raman spectra of amorphous materials such as silicate glass and melt. Although this conclusion does not rule out other solutions, it is consistent with available data and will be used in this report.

Effect of temperature-quenching

From infrared and Raman spectroscopic studies of silicate melts at high temperature (e.g., Sweet and White; 1969; Sharma et al., 1978; Seifert et al., 1981b), it has been concluded that in general, the overall spectral features of the high-temperature spectra of liquids closely resemble those of the quenched materials (glass) formed with quenching rates on the order of several hundred degrees Celsius per second. It was concluded, therefore, that average structural features of liquids and their quenched equivalent (glass) exhibit many similarities. This conclusion notwithstanding, recent high-temperature calorimetric data (e.g., Stebbins et al., 1984; Richet and Bottinga, 1986; Navrotsky et al., 1989) have shown ΔC_P values associated with the glass transition around 100 J/(mol·K). Stebbins (1988) summarized high-temperature ^{29}Si NMR data and concluded that equilibria of the form

$$2Q^m \leftrightarrow Q^{m-1} + Q^{m+1} \; (4 > m > 0), \quad (4)$$

often used to describe anionic equilibria in silicate melts, may shift systematically to the right with increasing temperature. He suggested that the in situ, high-temperature Raman data in the system Na_2O-Al_2O_3-SiO_2 (Seifert et al., 1981b) could be interpreted similarly.

In order to assess whether the qualitative interpretation of those data might be quantitatively accurate, the high-temperature Raman spectra from Seifert et al. (1981b) of liquid with bulk NBO/T = 1 and Al/(Al + Si) = 0.15 (NS2A15) have been deconvoluted according to the procedure outlined above with the resulting molar abundances of SiO_2 (Q^4), $Si_2O_5^{2-}$ (Q^3), and SiO_3^{2-} (Q^2) units shown in Table 3. The equilibrium constant for the reaction

$$Si_2O_5^{2-} \; (2Q^3) \leftrightarrow SiO_3^{2-} \; (Q^2) + SiO_2 \; (Q^4), \quad (5)$$

is shown as a function of temperature in Figure 4. Also plotted in this figure is the data point derived from the quenched melt, with the temperature of equilibration assumed equal to that of the glass transition. The latter temperature was used because it has recently been suggested (Brandriss and Stebbins, 1988) that in temperature-quenched melts, the unit distribution at the fictive

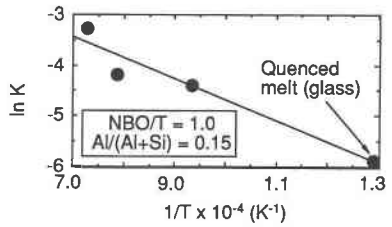

Fig. 4. Equilibrium constant for the equilibrium, $T_2O_5^{2-} \leftrightarrow TO_3^{2-} + TO_2$, as a function of temperature from the data shown in Table 3. Also shown is the data point for temperature-quenched NS2A15. The data point was plotted at the temperature of the glass transition point with the assumption that during quenching the unit distribution is quenched in at a temperature near the glass transition temperature.

temperature is reflected in the glass. The fictive temperature tends to be slightly higher than that of the glass transition, but in the absence of accurate information on its value, this temperature has been approximated by that of the glass transition.

A straight line through the four data points (including that of the glass as noted in Figure 4), indicates that (1) there is a distinctive temperature effect on the unit distribution at 1-bar pressure and (2) in quenched melts (glass), the unit distribution is frozen in near the glass transition. From the fit of the four data points, enthalpy and entropy of 34 ± 6 kJ/mol and 5 ± 6 J/(mol·K), respectively, for Reaction 5 was obtained. Although these values are somewhat uncertain, they accord with the values reported by Brandriss and Stebbins (1988) for a similar reaction obtained from high-temperature ^{29}Si NMR spectroscopy. Consequently, the structural data in the present report should be considered to be quantitatively applicable only at temperatures near those of the glass transition.

Results

The Raman spectra of the quenched melts, corrected for temperature- and frequency-dependent scattering intensity, are shown in Figures 5–7. The spectra of Al-free samples (Figs. 5A–7A) exhibit a characteristically intense, asymmetric envelope with a maximum near 1100 cm^{-1}, together with weaker and broader envelopes or shoulders near 800 cm^{-1}, 600 cm^{-1}, and 500 cm^{-1} (marked with arrows in the figures). The spectra are similar to other equivalently polymerized alkali and alkaline-earth silicate glasses (e.g., Brawer and White, 1975; Furukawa et al., 1981; Matson et al., 1983; McMillan and Piriou, 1983, Mysen et al., 1982b).

The spectra of $Li_2Si_4O_9$ (LS4), $Na_2Si_4O_9$ (NS4), and $K_2Si_4O_9$ (KS4) glasses differ in detail in that with decreasing ionic radius of the metal cation (Z/r^2 increases), the envelope near 800 cm^{-1} becomes more intense and the intensity of the 500 cm^{-1} envelope decreases relative to that of the 600 cm^{-1} envelope. Furthermore, whereas there is a distinct band near 950 cm^{-1} in the spectrum of

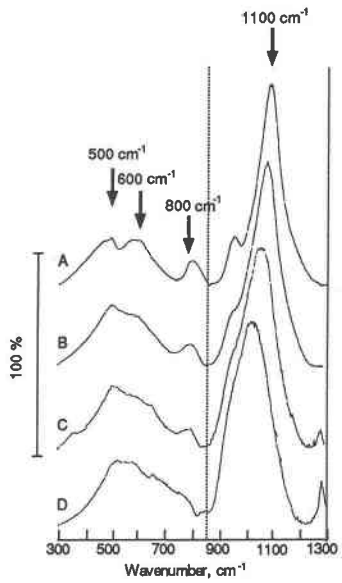

Fig. 5. Unpolarized Raman spectra, corrected for temperature- and frequency-dependent scattering intensity for quenched melts on the join $Li_2Si_4O_9$ (LS4)–$Li_2(LiAl)_4O_9$ (LA4) for (**A**) 0 mol%, (**B**) 10 mol%, (**C**) 20 mol%, and (**D**) 30 mol% LA4 component substituted for LS4.

$Li_2Si_4O_9$ glass (Fig. 5A), there is only a shoulder near this frequency for the $Na_2Si_4O_9$ glass (Fig. 6A). The Raman spectrum of $K_2Si_4O_9$ glass (Fig. 7A) shows little or not intensity in this frequency region.

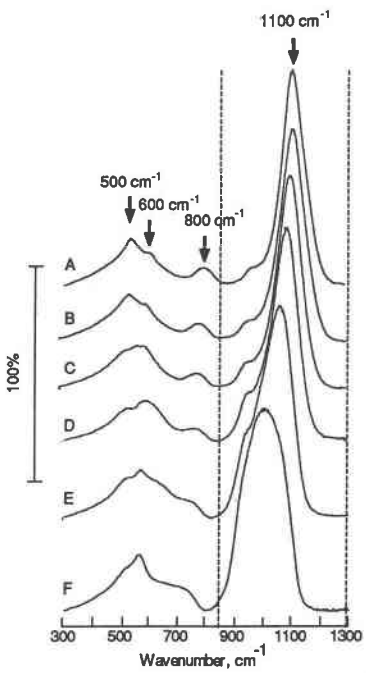

Fig. 6. Unpolarized Raman spectra, corrected for temperature- and frequency-dependent scattering intensity for quenched melts on the join $Na_2Si_4O_9$ (NS4)–$Na_2(NaAl)_4O_9$ (NA4) for (**A**) 0 mol%, (**B**) 5 mol%, (**C**) 10 mol%, (**D**) 20 mol%, (**E**) 30 mol%, and (**F**) 40 mol% NA4 component substituted for NS4.

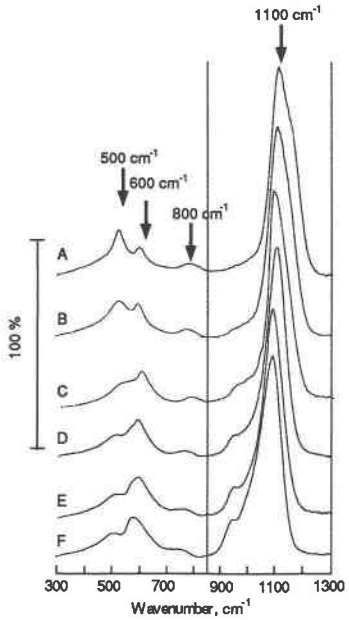

Fig. 7. Unpolarized Raman spectra, corrected for temperature- and frequency-dependent scattering intensity for quenched melts on the join $K_2Si_4O_9$ (KS4)–$K_2(KAl)_4O_9$ (KA4) for (**A**) 0 mol%, (**B**) 5 mol%, (**C**) 10 mol%, (**D**) 15 mol%, (**E**) 20 mol%, and (**F**) 25 mol% KA4 component substituted for KS4.

Substitution of charge-balanced Al for Si in these glasses results in a shift in frequency of the maximum of the 1100 cm^{-1} envelope to lower values (Figs. 5 and 6). Furthermore, whereas the spectrum of Al-free $K_2Si_4O_9$ glass does not exhibit any spectral signatures near 950 cm^{-1}, a shoulder grows in this frequency region as $(KAl)^{4+}$ substitutes for Si^{4+} (Fig. 7, B–F). Intensity increases near 950 cm^{-1} with increasing Al/(Al + Si) can also be discerned visually in the spectra of the glasses on the join $Li_2Si_4O_9$–$Li_2(LiAl)_4O_9$ (LS4–LA4) and $Na_2Si_4O_9$–$Na_2(NaAl)_4O_9$ (NS4–NA4) (Figs. 5–6) although this change in spectral topology is partially masked by the downward frequency shift of the high-frequency envelope as the melts become Al-rich. (see, in particular, Figs. 5B–5D, 6E, and 6F).

Thus, the Raman spectra of glasses on the three joins visually exhibit systematic changes as a function of Al/(Al + Si). In order to address these spectral changes in more detail, the high-frequency envelopes (between about 850 and 1300 cm^{-1} as marked in Figs. 5–7) have been curve-fitted (as described above) into their individual bands (Figs. 8–10). For convenience, with increasing frequency (in the Al-free systems), these bands are denoted ν_1 (~950 cm^{-1}), ν_2 (~1050 cm^{-1}), ν_3 (~1100 cm^{-1}), ν_4 (~1150 cm^{-1}), and ν_5 (~1200 cm^{-1}).

The intensities and frequencies of the Raman bands in the high-frequency envelope in spectra from glasses on each of the three joins change as systematic functions of bulk melt Al/(Al + Si) (Figs. 11 and 12). In the spectra of Al-free samples (Figs. 8A–10A), a narrow, strong peak (full width at half height, FWHH, <40 cm^{-1}) near 1100 cm^{-1} (ν_3) dominates the high-frequency envelope. Its area relative to the overall area of the high-frequency envelope is strongest for the KS4 composition (Fig. 10A) and weakest for the LS4 composition (Fig. 8A). The 950 cm^{-1} band (ν_1) is strongest in the spectrum of LS4 glass and weakest in KS4 glass.

The frequencies of the individual bands in the high-frequency envelopes are systematic functions of the bulk melt Al/(Al + Si) (Fig. 11) although the details of these relationships depend on the alkali metal. In the system $Li_2Si_4O_9$-$Li_2(LiAl)_4O_9$ (Fig. 11A), all the bands shift to lower frequency with increasing Al/(Al + Si). In the equivalent Na- and K-bearing systems (Fig. 11B and C), the ν_2, ν_4, and ν_5 band frequencies decrease systematically with increasing Al/(Al + Si), but significant Al substitution for Si is required [Al/(Al + Si) > 0.1] before an effect on the frequencies of the ν_1 and ν_3 bands can be observed. In the system $Na_2Si_4O_9$-$Na_2(NaAl)_4O_9$ (Fig. 11B), the frequency of the ν_3 band (1100 cm^{-1}) does not change until the bulk metal Al/(Al + Si) is between 0.1 and 0.2, in contrast to the equivalent Li-bearing system where the ν_3 band shifts by about 10 cm^{-1} per 0.1 unit change in Al/(Al + Si) over the entire compositional range (Fig. 11A). Similar relationships between Raman frequency and Al/(Al + Si) have been observed in the spectra of glasses in the system $K_2Si_4O_9$-$K_2(KAl)_4O_9$ (Fig. 11C). It appears, though, the bulk melt Al/(Al + Si) $\geq$ 0.2 is required before there are significant effects on the ν_1 and ν_3 band frequencies. Furthermore, the rate of frequency decrease of these bands with increasing Al/(Al + Si) is smaller in the K-bearing than in the Na-bearing system.

The principal variations in intensity (area) among the bands in the high-frequency envelope are seen for ν_1 and ν_3 (Fig. 12). In Figure 12, the equivalent areas are denoted A_1 (~950 cm^{-1}), A_2 (~1050 cm^{-1}), A_3 (~1100 cm^{-1}), A_4 (~1150 cm^{-1}), and A_5 (~1200 cm^{-1}). The general trends are similar for all compositions (different alkali metals) with the intensity, A_3, decreasing relative to $A_3 + A_4 + A_5$ and A_1 increasing relative to $A_1 + A_3$ as the melts become more aluminous. These intensities are, however, more sensitive to Al/(Al + Si) in the K-bearing system (Fig. 12C) than in either the Na- or the Li-bearing system. Those in the Na-bearing system (Fig. 12B) are more sensitive than those in the Li-bearing system (Fig. 12A). For example, for melts in the Al/(Al + Si) range between 0 and 0.2, the $A_3/(A_3 + A_4 + A_5)$ ratio decreases from 0.6 to 0.3, from 0.55 to 0.15, and from 0.6 to 0.05, and the $A_1/(A_1 + A_3)$ ratio increases from 0.2 to 0.4, from 0.1 to 0.4 and from 0 to 0.7 for the systems LS4-LA4 (Fig. 12A), NS4-NA4 (Fig. 12B), and KS4-KA4 (Fig. 12C), respectively.

Structural interpretation

The structural interpretation of Raman spectra of alkali silicate melts and glasses (e.g., Brawer and White, 1975; Verweij, 1979a, 1979b; Virgo et al., 1980; Furukawa et al., 1981; McMillan et al., 1982; Matson et al., 1983;

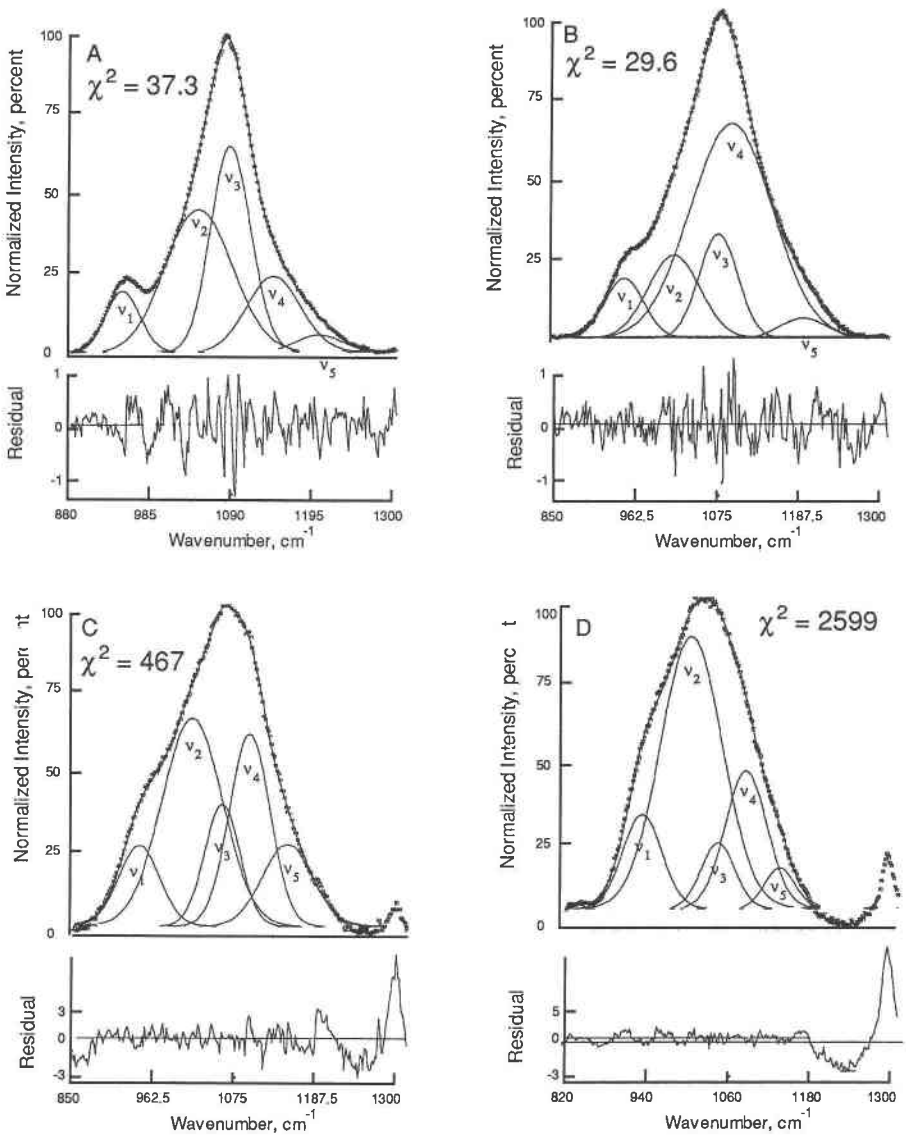

Fig. 8. Curve-fitted high-frequency region of the spectra in Fig. 5.

Mysen et al., 1982b; Domine and Piriou, 1986) generally accord with information from ^{29}Si and ^{27}Al NMR (e.g., Murdoch et al., 1985; Kirkpatrick et al., 1986; Stebbins, 1987) and X-ray data (e.g., DeJong et al., 1981; Imaoka et al., 1983). As originally suggested by Morey and Bowen (1924) on the basis of liquidus phase relations in alkali silicate systems, the melt structure inferred from the spectroscopic data can be considered in terms of a limited number of coexisting structural units (Virgo et al., 1980). These units are characterized by their number of nonbridging oxygens per Si. The units that have been identified are fully depolymerized (NBO/Si = 0), and units with NBO/Si = 0, 1, 2, 3, and 4 (or Q^4, Q^3, Q^2, Q^1 and Q^0, respectively).

In the Raman spectra of silicate melts and glasses, the Si-O^-(O^- = nonbridging oxygen) stretch bands in the high-frequency envelope (Figs. 8–10) show systematic frequency increases with decreasing NBO/Si of a particular structural unit. For units with NBO/Si = 4, this band is near 850 cm^{-1}. More polymerized structural units have their equivalent Si-O^- stretch bands near 900 cm^{-1} (NBO/Si = 3), 950 cm^{-1} (NBO/Si = 2), and near 1100 cm^{-1} (NBO/Si = 1) (e.g., Brawer and White, 1975; Virgo et al., 1980; Furukawa et al., 1981; Mysen et al., 1982b; McMillan, 1984). For structural units with NBO/Si < 4, there is also a mixed bending and stretching mode resulting in a Raman band between 600 and 700 cm^{-1} (Furukawa et al., 1981), the frequency of which depends on the Si-O-Si angle in the unit. This angle, in turn, decreases as the structural unit of interest becomes more

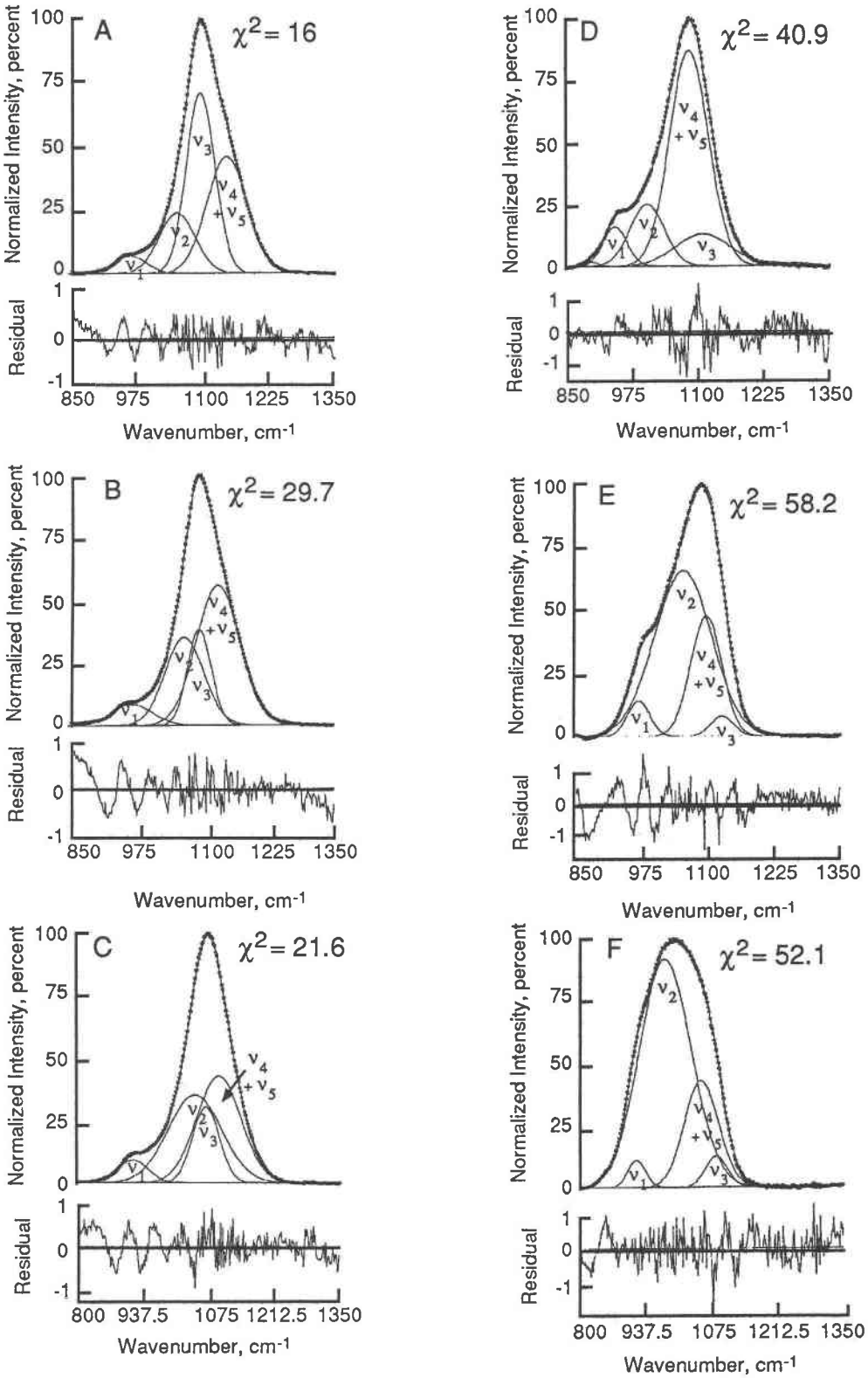

Fig. 9. Curve-fitted high-frequency region of the spectra in Fig. 6.

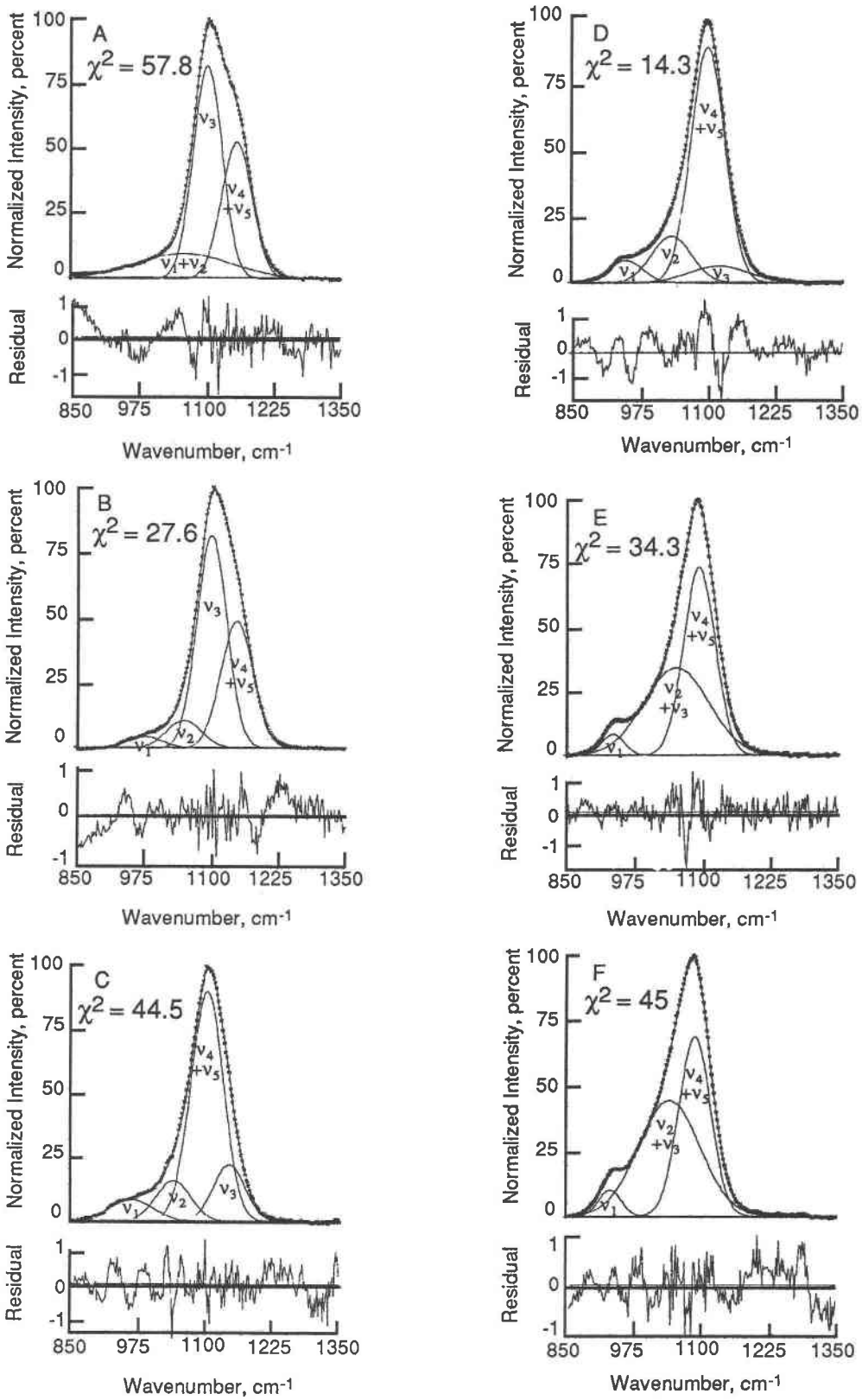

Fig. 10. Curve-fitted high-frequency region of the spectra in Fig. 7.

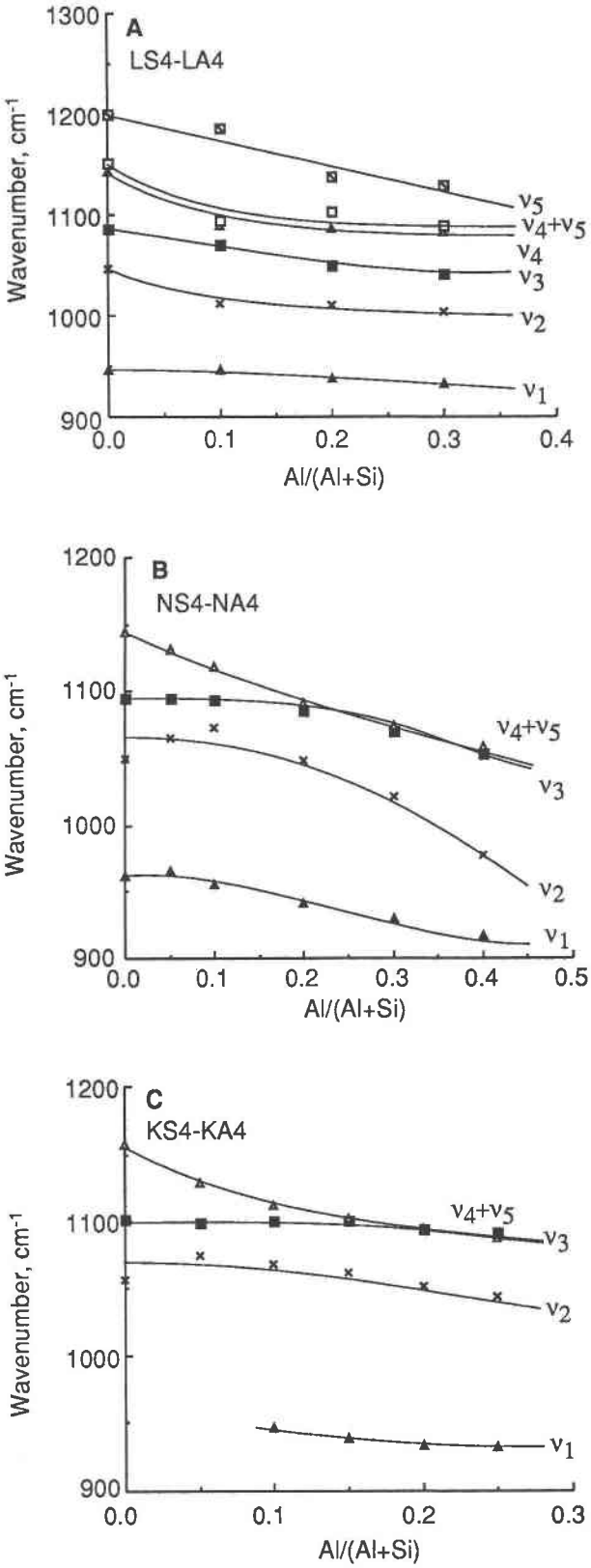

Fig. 11. Frequency shifts of Si-O stretch bands as a function of bulk-melt Al/(Al + Si).

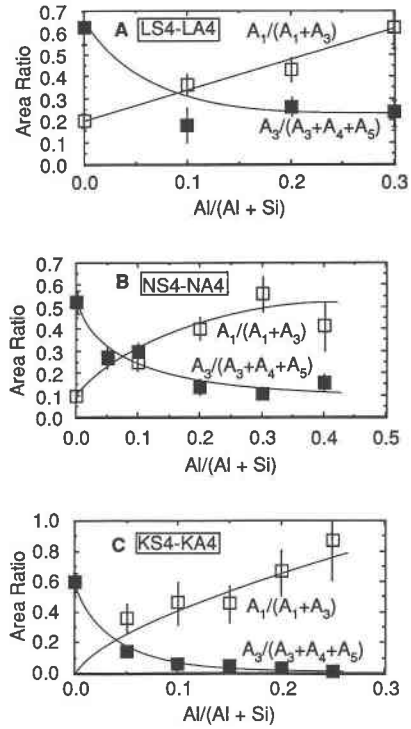

Fig. 12. Relative intensities of Si-O stretch bands (from Figs. 8–10) as a function of bulk-melt Al/(Al + Si).

depolymerized so that the band is near 600 cm^{-1} for units with NBO/Si = 1 and near 700 cm^{-1} for units with NBO/Si = 3 (see also Lazarev, 1972).

In addition to Raman bands associated with nonbridging oxygen, Raman bands due to Si-O^0 (O^0 = bridging oxygen) bonds are evident. For any structural unit that contains bridging oxygen, a stretch band near 1050 cm^{-1} appears (see also Lasaga, 1982). Moreover, whenever three-dimensionally interconnected network units exist in a melt, the Si-O^0 bonds from such units are manifested in one or two antisymmetric stretch bands between ~1150 (ν_4) and ~1200 cm^{-1} (ν_5). These latter two bands are not always resolved and in the spectra of quenched metal oxide–alumina–silica melts such as discussed in this report, the two bands often merge into one (referred to as $\nu_4 + \nu_5$). These bands tend to become difficult to resolve statistically in many of the spectra of Al-bearing quenched melts in part because of their apparently different frequency dependence on Al/(Al + Si) and in part because their relative intensities might be a function of the Al/(Al + Si) of the melts. In fully polymerized aluminate-silica melts (e.g., Seifert et al., 1982), such variations have been used to infer that perhaps two (or more) three-dimensionally interconnected structural units coexist. Their relative abundance and Al/(Al + Si) contents are functions of the bulk melt Al/(Al + Si) and the electronic properties of the charge-balancing cations. Although similar structural features might also exist in the three-dimensional structural units in the depolymerized aluminosilicate melts

discussed here, the spectra statistically generally do not permit such a detailed analysis.

In the spectra of aluminum-free lithium, sodium, and potassium silicate melts, Raman bands assigned to SiO_3^{2-} (Q^2), $Si_2O_5^{2-}$ (Q^3), and SiO_2 (Q^4) units can be identified (Figs. 5–10). The band near 1100 cm^{-1} (ν_3) is assigned to Si-O^- stretching in a structural unit with NBO/Si = 1 (Q^1 or $Si_2O_5^{2-}$ units). The bands near 1150–1200 cm^{-1} (ν_4 and ν_5) result from the presence of three-dimensional network units (Q^4 or SiO_2 units). The band or shoulder near 950 cm^{-1} (ν_1) is assigned to Si-O^- stretching in a structural unit with NBO/Si = 2 (Q^2 or SiO_3^{2-} units). The broader band near 600 cm^{-1} is assigned to the mixed stretch and bending modes in mixtures of $Si_2O_5^{2-}$ and SiO_3^{2-}. The anionic structure of Al-free tetrasilicate melts is, therefore, viewed as mixture of three-dimensionally interconnected structural units, together with units with NBO/Si = 1 and units with NBO/Si = 2. For Al-free tetrasilicate melts, Reaction 5 adequately describes, therefore, the anionic equilibrium. This conclusion accords with those from other Raman and NMR data for melts and glasses in the same polymerization range (e.g., Virgo et al., 1980; Mysen et al., 1980, 1982b; Matson et al., 1983; Murdoch et al., 1985; Kirkpatrick et al., 1986; Stebbins, 1987, 1988).

Substitution of Al^{3+} for Si^{4+} with concomitant Li, Na, or K charge-balancing has two principal spectral effects. The intensity relations among the bands change, and the frequencies of some of the diagnostic bands are affected. There is no evidence for additional bands in the spectra as the Al content of the melts is increased. Thus, a reaction analogous to Reaction 5 can be written for the anionic equilibrium in the aluminosilicate melts by replacing Si in Reaction 5 with T [where T = Si^{4+} + $(MAl)^{4+}$; M = alkali metal].

The Al-dependent frequencies of the high-frequency Raman bands (Figs. 8–10) may be related to Al substitution for Si in the structural units. The ν_4 and ν_5 band frequencies are lowered with increasing bulk-melt Al/(Al + Si), whereas those of the ν_1 and ν_3 bands are less sensitive to Al contents (Fig. 11). The frequency decreases either result from (Si,Al) coupling or a decrease in the force constant resulting from the weakening of the T-O bonds as Al is substituted for Si, or both. In either case, the frequency reductions reflect substitution of Al^{3+} for Si^{4+} in tetrahedral coordination. With less than 10%–20% Al in substitution for Si in the Na- and K-bearing systems, the frequencies of these two bands do not vary with Al/(Al + Si), but they do show a decrease as the Al contents are increased further. The greater sensitivity of the SiO^0 stretch-band (ν_4 + ν_5) frequencies as compared with those of the Si-O^- stretch bands (ν_1 and ν_3) might reflect a preference of the Al^{3+} for the most polymerized structural unit (TO_2 or Q^4) relative to structural units that contain nonbridging oxygen ($T_2O_5^{2-}$ and TO_3^{2-}, or Q^3 and Q^2; see also Mysen et al., 1981, 1985). This conclusion is consistent with ^{27}Al and ^{29}Si NMR spectroscopy of melts of similar compositions (e.g., Engelhardt et al., 1985; Kirkpatrick et al., 1986) as well as other Raman data (Domine and Piriou, 1986) indicating, therefore, that the Q^4 unit (NBO/Si = 0) is a principal location for Al^{3+} in the melts relative to Q^3 (NBO/Si = 1) and Q^2 (NBO/Si = 2) units.

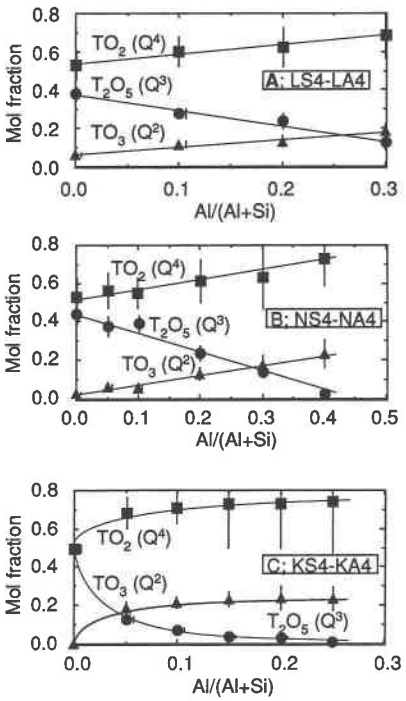

Fig. 13. Relative abundance of structural units as a function of bulk-melt Al/(Al + Si) for the systems indicated.

Mysen et al. (1981, 1985) suggested that the preference of Al for fully polymerized structural units could be rationalized by analogy with crystal-chemical data from aluminosilicate minerals. In such silicates, Al shows a distinct preference for the tetrahedral site neighboring the oxygen bridge with the smallest intertetrahedral angle (e.g., Brown et al., 1969). Among the three coexisting structural units dominating the structure of the aluminum-bearing alkali tetrasilicate melts, from geometric considerations it is most likely that the fully polymerized unit in a given system has the smallest average intertetrahedral angle (Furukawa et al., 1981). Thus, a preference by Al^{3+} for such units would be expected in accord with the structural interpretation of the Raman spectra.

Composition-abundance relations

The intensities of Si-O^- stretch bands (ν_1 and ν_3) from the deconvoluted, high-frequency envelopes of the spectra can be used to estimate the relative abundances of the structural units in the melts as discussed above. The results of these calculations are shown in Figure 13. In all three systems, the abundance of T_2O_5 (Q^3) units decreases, and the abundances of TO_2 (Q^4) and TO_3 (Q^2) units increase systematically as a function of increasing Al/(Al + Si) of the melt. As no other structural units can

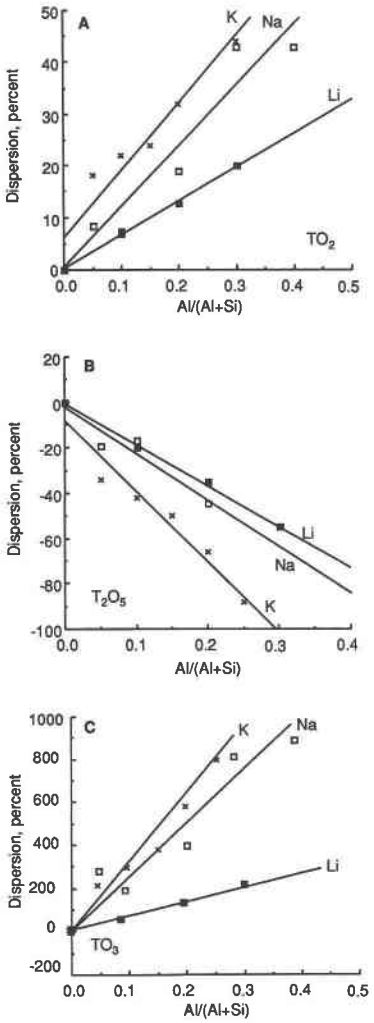

Fig. 14. Dispersion of structural-unit abundance as a function of bulk-melt Al/(Al + Si) for the systems and units indicated.

be identified in the melts, this observation implies that substitution of Al for Si with alkali charge-balancing shifts Reaction 5 to the right.

The rate of change of unit abundance with Al substitution, relative to the Al-free end-member, will be referred to as dispersion. The dispersion is more pronounced for metal cations of Z/r^2 (Fig. 14). Thus, the effect of Al substitution on the relative abundance of the structural units is greatest for the K-bearing system and least evident for the Li-bearing system. This observation, in turn, may be related to the extent to which the intertetrahedral angles in the coexisting units depend on the network-modifying metal cation. From crystal chemistry (e.g., Liebau, 1981), sheets and chains in crystalline silicates become increasingly puckered as the network-modifying cation becomes smaller or more highly charged, or both. It is suggested here that in silicate melts, this puckering or distortion of the structural units with increasing Z/r^2 of the metal cation may result in smaller average differences in intertetrahedral angle between the coexisting structural units. Because the Al distribution between the structural units appears related to this angle, by diminishing the angle difference between the structural units, it is likely that the Al preference for a given structural unit is less pronounced. This rationale may be employed, therefore, to explain the decreasing degree of dispersion of Al with increasing Z/r^2 of the metal cation. For a given bulk-melt Al/(Al + Si), the Al probably is partitioned more strongly into the fully polymerized network units (TO_2 or Q^4) as Z/r^2 of the metal cation decreases, as also indicated by the systematic variations in the shifts in the Raman frequencies as a function of Al/(Al + Si) discussed above (Fig. 11). Because enhanced abundance of TO_2 units also requires an increase in TO_3 abundance (in order to maintain mass balance), it is suggested that this behavior of Al is a principal driving force behind the enhanced dispersion (Fig. 14) as the Z/r^2 of the metal cation is lowered.

TABLE 4. Bulk compositional and structural information for tholeiite and nepheline-normative melt composition

Parameter	Tholeiite (1092 analyses)	Nepheline-normative basalt (233 analyses)
Al/(Al + Si)	0.267 ± 0.028	0.274 ± 0.032
NBO/T	0.688 ± 0.257	0.867 ± 0.272
TO_3 (Q^2)	0.215 ± 0.057	0.252 ± 0.061
T_2O_5 (Q^3)	0.012 ± 0.002	0.015 ± 0.009
TO_2 (Q^4)	0.687 ± 0.094	0.589 ± 0.095
$M^+(TO_2)$*	0.586 ± 0.081	0.619 ± 0.126
$M^{2+}(TO_2)$*	0.413 ± 0.081	0.379 ± 0.115
Al/(Al + Si)(TO_2)	0.389 ± 0.048	0.465 ± 0.057

Note: Data base: Rockfile RKNFSYS for Cenozoic extrusive igneous rocks compiled by Chayes (1975a, 1975b; 1985 version NTRM2 is unpublished).
* Proportion of Al^{3+} in TO_2 units charge-balanced with alkali metals (M^+) or alkaline earths (M^{2+}).

APPLICATIONS

Transport properties of silicate melts (e.g., viscosity, diffusivity, and conductivity) can be correlated with the abundance of fully polymerized structural units (e.g., Dingwell, 1986) and also with the strength of the bridging T-O bond. On the one hand, substitution of Al for Si in tetrahedral coordination will weaken the bond. This weakening is more pronounced the smaller the charge-balancing cation (as suggested, for example, by the heat-of-solution data for melts on SiO_2–$MAlO_2$ joins; see Navrotsky et al., 1985). In melts where Al^{3+} substitution does not affect the proportions of other structural units, the weakening of the T-O bonds is likely to enhance the diffusivity, conductivity, and fluidity of the melt. The Al substitution in depolymerized silicate melts also results, however, in enhancement of the proportion of three-dimensional network units because of the preference of Al^{3+} for the three-dimensional network unit. This preference is more pronounced the larger the charge-balancing cat-

ion. Thus, the abundance increase of three-dimensional network units is greater the larger the charge-balancing alkali metal. Increased abundance of three-dimensional network units will result in decreasing values of fluidity and diffusivity. Although Al substitution for Si in fully polymerized silicate melts results in a lowering of the viscosity and an increase in diffusivity and conductivity, it is, thus, possible that the concomitant increase in abundance of TO_2 units, resulting from this substitution in depolymerized melts, could reverse these trends. The likelihood that this reversal occurs for a given bulk-melt degree of polymerization is greater the larger the alkali metal.

One might speculate that properties of silicate melts that are sensitive to both the abundance of three-dimensional network units in the melts and to the strength of bridging T-O bonds (T = Si,Al) are significantly dependent on the type of charge-balancing and network-modifying cation even at the same Al/(Al + Si) and M/(Al + Si) (M = metal cation). For example, the compressibility and thermal expansion of silicate melts are primarily governed by the abundance of TO_2 units (see Tomlinson et al., 1958, and Bockris and Kojonen, 1960, for relevant experimental data). For aluminosilicate melts with the same bulk-melt degree of polymerization and the same Al/(Al + Si), the values of these parameters are, therefore, likely to be greater for potassium aluminosilicate melts than for sodium aluminosilicate melts and greater for sodium aluminosilicate melts than for lithium aluminosilicate melts. This trend is expected because the abundance of TO_2 units in the depolymerized aluminosilicate melts increases the smaller the Z/r^2 of the metal cation. This suggestion may explain, for example, why nepheline-normative basalt melts are more compressible than tholeiite melts even though the overall Al/(Al + Si) ratios of these groups of rocks are similar and the average NBO/T of nepheline-normative basalts is slightly higher than that of tholeiite (Table 4). In alkali basalts, a greater fraction of the tetrahedrally coordinated Al^{3+} is charge-balanced by alkali metals (Na and K) than in olivine tholeiite. Furthermore, the Al/(Al + Si) ratio of the three-dimensionally interconnected units (TO_2) in melts of nepheline-normative basalt is also significantly higher than in tholeitte (Table 4). Thus, both the abundance of TO_2 units and the compressibility of these units are likely to be greater in alkali basalt than in olivine tholeiite.

Acknowledgments

The manuscript was prepared while I was in residence at the Bayerisches Geoinstitut, Universität Bayreuth, during the summer of 1988. The support and hospitality enjoyed during this stay are appreciated. Critical reviews by F. A. Seifert and C. T. Prewitt are greatly appreciated.

References cited

Barker, A.S., and Sievers, A.S. (1975) Optical studies of the vibrational properties of disordered solids. Reviews in Modern Physics, 47, 1–169.

Bockris, J.O'M., and Kojonen, F. (1960) The compressibility of certain molten alkali silicates and borates. Journal of the American Ceramic Society, 82, 4493–4497.

Bockris, J.O'M., Mackenzie, J.O., and Kitchner, J.A. (1955) Viscous flow in silica and binary liquid silicates. Transactions on the Faraday Society, 51, 1734–1748.

Bottinga, Y., Richet, P., and Weill, D.F. (1983) Calculation of the density and thermal expansion coefficient of silicate liquids. Bulletin Minéralogique, 106, 129–138.

Brandriss, M.E., and Stebbins J.F. (1988) Effects of temperature on the structures of silicate liquids, ^{29}Si NMR results. Geochimica et Cosmochimica Acta, 52, 2659–2669.

Brawer, S. A., and White, W.B. (1975) Raman spectroscopic investigation of the structure of silicate glasses. I. The binary silicate glasses. Journal of Chemical Physics, 63, 2421–2432.

Brown, G.E., Gibbs, G.V., and Ribbe, P.H. (1969) The structure and variation in the length of Si-O and Al-O bonds in framework silicates. American Mineralogist, 54, 1044–1061.

Chayes, F. (1975a) Average composition of the commoner Cenozoic volcanic rocks. Carnegie Institution of Washington Year Book 74, 547–549.

——— (1975b) A world data base for igneous petrology. Carnegie Institution of Washington Year Book 74, 549–550.

Davidon, W.C. (1966) Variable metric method for minimization (3rd revision). Lawrence Livermore, Argonne National Laboratory ANL 5990.

DeJong, B.H.W.S., Keefer, K.D., and Brown, G.E. (1981) Polymerization of silicate and aluminate tetrahedra in glasses, melts and aqueous solutions. III—Local silicon environments and internal nucleation in silicate glasses. Geochimica et Cosmochimica Acta, 44, 1627–1643.

Dingwell, D.B. (1986) Viscosity-temperature relationships in the system $Na_2Si_2O_5$-$Na_4Al_2O_5$. Geochimica et Cosmochimica Acta, 50, 1261–1265.

Domine, F., and Piriou, B. (1986) Raman spectroscopic study of the SiO_2-Al_2O_3-K_2O vitreous system: Distribution of silicon and second neighbors. American Mineralogist, 71, 38–50.

Eliezer, N., Howald, R.A., Marinkovic, M., and Eliezer, I. (1978) Vapor pressure measurements, thermodynamic parameters, phase diagram in the system potassium oxide–silicon oxide at high temperature. Journal of Chemical Physics, 82, 1021–1028.

Eliezer, N., Eliezer, I., Howald, R.A., Verwolf, M.C., and Viswanadam, P. (1979) The enthalpy of sodium silicate glasses and liquids. CALPHAD, 3, 1–8.

Engelhardt, G., Nofz, M., Forkel, K., Wishmann, F.G., Magi, M., Samoson, A., and Lippmaa, E. (1985) Structural studies of calcium aluminosilicate glasses by high resolution solid state ^{29}Si and ^{27}Al magic angle spinning nuclear magnetic resonance. Physics and Chemistry of Glasses, 26, 157–165.

Fletcher, R., and Powell, M.J.D. (1963) A rapidly converging descent method for minimization. Computer Journal, 6, 163–168.

Furukawa, T., Fox, K.L., and White, W.B. (1981) Raman spectroscopic investigation of the structure of silicate glasses. III. Raman intensities and structural units in sodium silicate glasses. Journal of Physical Chemistry, 15, 3226–3237.

Hartwig, C.M. (1977) The radiation-induced formation of hydrogen and deuterium compounds in silica as observed by Raman scattering. Journal of Chemical Physics, 66, 227–239.

Imaoka, M., Hasegawa, H., and Yasui, I. (1983) X-ray diffraction study of the structure of silicate glasses. Part 2. Alkali disilicate glasses. Physics and Chemistry of Glasses, 24, 72–78.

Kirkpatrick, R.J., Oestrike, R., Weiss, C.A., Smith, K.A., and Oldfield, E. (1986) High-resolution ^{27}Al and ^{29}Si NMR spectroscopy of glasses and crystals along the join $CaMgSi_2O_6$–$CaAl_2SiO_6$. American Mineralogist, 71, 705–711.

Lasaga, A.C. (1982) Optimization of CNDO for molecular orbital calculation on silicates. Physics and Chemistry of Minerals, 8, 36–46.

Lazarev, A.N. (1972) Vibrational spectra and structure of silicates. New York, Consultants Bureau.

Liebau, F. (1981) The influence of cation properties on the conformation of silicate and phosphate anions. In (M. O'Keefe and A. Navrotsky, Eds., Structure and bonding in crystals, p. 197–232. Academic Press, New York.

Long, D.A. (1977) Raman spectroscopy. New York, McGraw-Hill.

Matson, D.W., Sharma, S.K., and Philpotts, J.A. (1983) The structure of

high-silica alkali-silicate glasses—A Raman spectroscopic investigation. Journal of Non-Crystalline Solids, 58, 323–352.

McKeown, D.A., Galeener, F.L., and Brown, G.E. (1984) Raman studies of Al-coordination in silica-rich sodium aluminosilicate glasses and some related minerals. Journal of Non-Crystalline Solids, 68, 361–378.

McMillan, P. (1984) A Raman spectroscopic study of glasses in the system CaO-MgO-SiO_2. American Mineralogist, 69, 645–659.

McMillan, P., and Piriou, B. (1983) Raman spectroscopic studies of silicate and related glass structure: A review. Bulletin Minéralogique, 106, 57–77.

McMillan, P., Piriou, B., and Navrotsky, A. (1982) A Raman spectroscopic study of glasses along the joins silica–calcium aluminate, silica–sodium aluminate and silica–potassium aluminate. Geochimica et Cosmochimica Acta, 46, 2021–2037.

Morey, G.W., and Bowen, N.L. (1924) The binary system sodium metasilicate–silica. Journal of Physical Chemistry, 28, 1167–1179.

Murdoch, J.B., Stebbins, J.F., and Carmichael, I.S.E. (1985) High-resolution ^{29}Si NMR study of silicate and aluminosilicate glasses: The effect of network-modifying cations. American Mineralogist, 70, 332–343.

Mysen, B.O. (1987) Magmatic silicate melts: Relations between bulk composition, structure and properties. In B.O. Mysen, Ed., Magmatic processes: Physiocochemical principles, p. 375–400. Geochemical Society Special Publication No. 1.

Mysen, B.O., and Virgo, D. (1985) Raman spectra and structure of fluorine- and water-bearing silicate glasses and melts. In J. Snyder, R.L. Condrate, and R.R. Johnson, Eds., Advances in materials characterization, p. 43–55. New York, Plenum Press.

Mysen, B.O., Virgo, D., and Scarfe, C.M. (1980) Relations between the anionic structure and viscosity of silicate melts—A Raman spectroscopic study. American Mineralogist, 65, 690–710.

Mysen, B.O., Virgo, D., and Kushiro, I. (1981) The structural role of aluminum in silicate melts—A Raman spectroscopic study at 1 atmosphere. American Mineralogist, 66, 678–701.

Mysen, B.O., Finger, L.W., Seifert, F.A., and Virgo, D. (1982a) Curve-fitting of Raman spectra of amorphous materials. American Mineralogist, 67, 686–696.

Mysen, B.O., Virgo, D., and Seifert, F.A. (1982b) The structure of silicate melts: Implications for chemical and physical properties of natural magma. Reviews of Geophysics, 20, 353–383.

Mysen, B.O., Virgo, D., and Seifert, F.A. (1985) Relationships between structure and properties of aluminosilicate melts. American Mineralogist, 69, 834–847.

Navrotsky, A., Geisinger, K.L., McMillan, P., and Gibbs, G.V. (1985) The tetrahedral framework in glasses and melts—Influences from molecular orbital calculations and implications for structure, thermodynamics and physical properties. Physics and Chemistry of Minerals, 11, 284–298.

Navrotsky, A., Ziegler, D., Oestrike, R., and Maniar, P. (1989) Calorimetry of silicate melts at 1773K, measurement of enthalpies of fusion and of mixing in the systems diopside-anorthite and anorthite-forsterite. Contributions to Mineralogy and Petrology, 101, 122–130.

Oestrike, R., and Kirkpatrick, R.J. (1988) ^{27}Al and ^{29}Si MASS NMR spectroscopy of glasses in the system anorthite-diopside-forsterite. American Mineralogist, 73, 534–546.

Powell, M.J.D. (1964a) A method for minimizing a sum of non-linear functions without calculating derivatives. Computer Journal, 7, 303–307.

——— (1964b) The efficient method for finding a minimum of a function of several variables without calculating derivatives. Computer Journal, 1, 155–162.

Richet, P., and Bottinga, Y. (1986) Thermochemical properties of silicate glasses and liquids.—A review. Reviews of Geophysics, 24, 1–26.

Robinson, H.A. (1969) Physical properties of alkali silicate glasses. I. Additive relations in alkali binary glasses. Journal of the American Ceramic Society, 53, 392–399.

Ryerson, F.J. (1985) Oxide solution mechanisms in silicate melts: Systematic variations in the activity coefficients of silica. Geochimica et Cosmochimica Acta, 49, 637–651.

Schneider, E., Stebbins, J.F., and Pines, A. (1987) Speciation and local structure in alkali and alkaline earth silicate glasses.—Constraints from ^{29}Si NMR spectroscopy. Journal of Non-Crystalline Solids, 89, 371–383.

Seifert, F.A., Mysen, B.O., and Virgo, D. (1981a) Quantitative determination of proportions of anionic units in silicate melts. Carnegie Institution of Washington Year Book 80, 301–302.

——— (1981b) Structural similarity between glasses and melts relevant to petrological processes. Geochimica et Cosmochimica Acta, 45, 1879–1884.

——— (1982) Three-dimensional network melt structure in the systems SiO_2-$NaAlO_2$, SiO_2-$CaAl_2O_4$ and SiO_2-$MgAl_2O_4$. American Mineralogist, 67, 696–718.

Sharma, S.K., Virgo, D., and Mysen, B.O. (1978) Structure of glasses and melts of $Na_2O \cdot xSiO_2$ (x = 1, 2, 3) composition from Raman spectroscopy. Carnegie Institution of Washington Year Book 77, 649–652.

Stebbins, J.F. (1987) Identification of multiple structural species in silicate glasses by ^{29}Si NMR. Nature, 330, 465–467.

——— (1988) Effects of temperature and composition on silicate glass structure and dynamics, Si-29 NMR results. Journal of Non-Crystalline Solids, 106, 359–369.

Stebbins, J.F., Carmichael, I.S.E., and Moret, L.K. (1984) Heat capacities and entropies of silicate liquids and glasses. Contributions to Mineralogy and Petrology, 86, 131–148.

Sweet, J.R., and White, W.B. (1969) Study of sodium silicate glasses and liquids by infrared spectroscopy. Physics and Chemistry of Glasses, 10, 246–251.

Tomlinson, J.W., Heynes, M.S.R., and Bockris, J.O,M. (1958) The structure of liquid silicates. Part 2. Molar volume and expansivities. Transactions of the Faraday Society, 54, 1822–1834.

Urbain, G., Bottinga, Y., and Richet, P. (1982) Viscosity of liquid silica, silicates and aluminosilicates. Geochimica et Cosmochimica Acta, 46, 1061–1072.

Verweij, H. (1979a) Raman study of the structure of alkali germanosilicates. I. Sodium and potassium metagermanosilicate glasses. Journal of Non-Crystalline Solids, 33, 41–53.

——— (1979b) Raman study of the structure of alkali germanosilicate glasses. II. Lithium, sodium and potassium digermanosilicate glass. Journal of Non-Crystalline Solids, 33, 55–69.

Virgo, D., Mysen, B.O., and Kushiro, I. (1980) Anionic constitution of silicate melts quenched at 1 atm from Raman spectroscopy: Implications for the structure of igneous melts. Science, 208, 1371–1373.

Walrafen, G.E. (1967) Raman spectral studies of the effects of temperature on water structure. Journal of Chemical Physics, 44, 114–126.

Manuscript received November 7, 1988
Manuscript accepted September 25, 1989